

Nonconservation of parity in atomic bismuth

G. N. Birich, Yu. V. Bogdanov, S. I. Kanorskii, I. I. Sobel'man, V. N. Sorokin, I. I. Struk, and E. A. Yukov

P. N. Lebedev Physics Institute, Academy of Sciences of the USSR, Moscow

(Submitted 13 April 1984)

Zh. Eksp. Teor. Fiz. **87**, 776–789 (September 1984)

Measurements are reported of the optical activity of bismuth vapor due to parity nonconservation in weak interactions between atomic electrons and nucleons of the nucleus in the $6p^3\ ^4S_{3/2} - 6p^3\ ^2D_{5/2}$, $\lambda = 648$ nm transition. The constant $R = \text{Im}(E1/M1)$ characterizes the size of the effect, and its value is found to be $(-7.8 \pm 1.8) \times 10^{-8}$.

INTRODUCTION

This paper reports an experimental search for the optical activity of the vapor of atomic bismuth. This effect is predicted by the Weinberg-Salam theory of electroweak interactions and arises from the parity-conserving weak interaction between atomic electrons and the nucleus (we shall refer to it as the PNC effect; see, for example, Refs. 1–6).

The measurements were performed on the $F = 6 \rightarrow F' = 7$ hyperfine-structure component of the magnetic dipole transition $6p^3\ ^4S_{3/2} \rightarrow 6p^3\ ^2D_{5/2}$, $\lambda = 648$ nm. The PNC effect is characterized by the constant

$$R = \text{Im}(E1/M1), \quad (1)$$

where $M1$ is the magnetic-dipole matrix element, $E1$ is the matrix element of the electric dipole due to the mixing of the odd $6s^2 6p^3$ state with even states of the form $6s^2 6p^2 ns$, $6s 6p^4$, and so on.

Our first measurements^{7,8} showed that

$$R = (-2.4 \pm 1.3) \cdot 10^{-8},$$

where the term 1.3×10^{-8} is the estimated standard deviation. Reduction of our data using the χ^2 criterion showed the average value $D = \pm 2.5 \times 10^{-8}$ lay within the 90% confidence interval and that the statistics deviate considerably from Gaussian. As noted in Ref. 8, the measurements were subject to instrumental uncertainties that were relatively slowly-varying functions of time.

A detailed study of possible instrumental uncertainties was undertaken in subsequent experiments, and a number of measures was taken to remove these uncertainties. New and much more extensive measurements were also carried out.

EXPERIMENTAL TECHNIQUE AND APPARATUS

The rotation of the plane of polarization associated with the $F = 6 \rightarrow F' = 7$ transition due to the PNC effect is related to the constant R in (1) by

$$\varphi_{\text{PNC}} = -0.89(4\pi/\lambda)(n-1)RL, \quad (2)$$

where L is the length of the column of bismuth vapor, n is the refractive index, the coefficient 0.89 is due to the fact that $\varphi_{\text{PNC}} \propto (M1)^2 R$, and the absorption and dispersion include contributions of not only $M1$ but also of the electric-quadrupole matrix element $E2$ (we used the ratio $E2/M1 = 0.60$, taken from Ref. 9, to calculate this coefficient).

Like the dispersion $n - 1$, the angle φ_{PNC} vanishes at the center of the line and has a maximum and a minimum at

the same points as the function $n(\omega)$, i.e., at approximately the half-width of the profile. The total difference between rotations at the points of maximum and minimum can be expressed in terms of the absorption coefficient κ (in cm^{-1}) at the center of the transition as follows:

$$\Delta\varphi_{\text{PNC}} = -0.89(4\pi/\lambda)(n_{\text{max}} - n_{\text{min}})RL = -0.89\xi R\kappa L. \quad (3)$$

The coefficient ξ depends on the ratio $\gamma/2\Delta\omega_D$, where γ is the collisional width and $\Delta\omega_D$ is the Doppler width. It turns out that $\xi = 1$ and $\xi = 1.22$ for the Lorentz and Doppler profiles, respectively.

Direct measurements of κL and $\gamma/2\Delta\omega_D$ are difficult in the case of the 648-nm transition because the absorption spectrum of atomic bismuth has superimposed upon it the absorption spectrum of bismuth molecules, which has roughly the same intensity. In our measurements, κL was determined from the bismuth-vapor Faraday rotation $\varphi_F(\omega, H_c) = \chi(\omega)LH_c$ for which the contribution of molecular lines is negligible in a given magnetic field H_c . The function $\varphi_F(\omega, H_c)$ has a maximum at the center of the line (near the absorption maximum and zero φ_{PNC}), and vanishes at the points ω_+ , ω_- which are practically coincident with the maximum and minimum of φ_{PNC} . The absorption coefficient at the line center is related to the Faraday rotation at the maximum by

$$\kappa L = \varphi_F^{\text{max}} / aH_c. \quad (4)$$

The constant a is determined by the Landé factors of the levels under consideration, the line profile, and the ratio $E2/M1$ (see, for example, Ref. 6). The necessary Landé factors were taken from Ref. 10 and the ratio $E2/M1 = 0.60$ was adopted in accordance with Ref. 9.

This determination of κL from the Faraday rotation has an important advantage. The precision with which the constant R in (3) can be determined is actually independent of the absolute calibration of the measured angles because

$$R \propto (\Delta\varphi_{\text{PNC}} / \varphi_F^{\text{max}}) H_c. \quad (5)$$

All that is required is to have an absolute calibration of the field H_c . The magnetic field is balanced out to zero during the measurements of $\Delta\varphi_{\text{PNC}}$. The quantities $\Delta\varphi_{\text{PNC}}$ and φ_F^{max} (in the residual field) are found from measurements of rotation at three spectral points, ω_+ , ω_- , and ω_0 , i.e., the zeros and the maximum of the Faraday rotation. This yields

$$\Delta\varphi_{\text{PNC}} = \varphi_+ - \varphi_-, \quad \varphi_F^{\text{max}} = 1/2[(\varphi_0 - \varphi_+) + (\varphi_0 - \varphi_-)]. \quad (6)$$

Measurements of φ_F^{max} simultaneously with $\Delta\varphi_{\text{PNC}}$ enable us

to monitor the residual magnetic field in the system.

Measurements of the rotation φ of the plane of polarization of the light wave are performed by a null method and by the classical modulation technique. The Faraday cell is placed between crossed polarizer and analyzer, and an alternating magnetic field of frequency $\Omega/2\pi = 1107$ Hz is applied to it together with an additional controlling field produced by the current i in a coil surrounding it, which gives rise to an additional rotation $\varphi_m \cos \Omega t + \delta(i)$. The result of this is that the plane of polarization of the light wave rotates through the angle

$$\Psi = \varphi + \varphi_m \cos \Omega t + \delta(i). \quad (7)$$

The amplitude of the signal wave at exit from the polarimeter is $E_c \propto \Psi$ and the intensity is proportional to Ψ^2 . The signal at the frequency Ω is proportional to $\varphi_m [\varphi + \delta(i)]$. This signal is isolated and is balanced out by a negative feedback loop carrying the signal produced by the controlling magnetic field. We then have

$$\varphi = -\delta(i). \quad (8)$$

The measurement of φ is thus reduced to the measurement of the current i .

A block diagram of the apparatus is shown in Fig. 1. The principal components of its optical part are the single-frequency laser, the polarimeter, and the furnace containing the bismuth vapor.

We employed the Spectra Physics 580 A laser using a solution of the AZhN 650 dye.¹⁾ The standard frequency-tuning system was augmented by a comparison system whereby the laser frequency was tied to external reference points, i.e., the maxima of the absorption spectrum, the maxima and zeros of the Faraday rotation profile, and the transmission peak of the inertial interferometer. The ar-

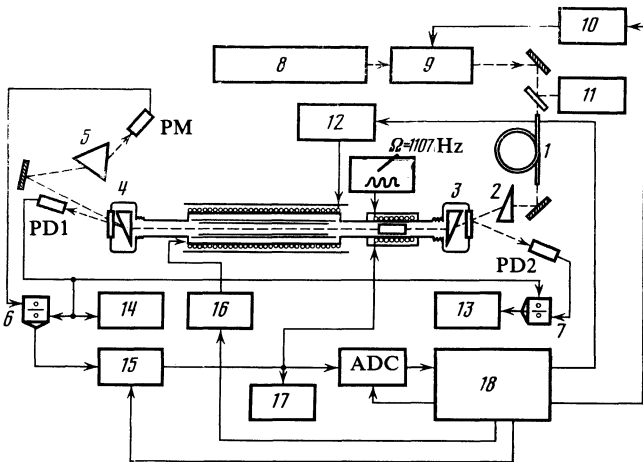


FIG. 1. Block diagram of the spectropolarimeter: 1—single-mode light guide (external diameter $120 \mu\text{m}$, internal diameter $4.5 \mu\text{m}$, $l = 1.6$ m, $\lambda_{\text{crit}} = 0.58 \mu\text{m}$); 2, 3, 4—calcite prisms (prism 2 is used to compensate the angular dispersion of the polarizer 3); 5—dispersing prism used to prevent the illumination of the photomultiplier by radiation from the furnace and to compensate the angular magnification of the analyzer 4; 6, 7— analog dividers used to normalize rotation and absorption signals; 8—Ar⁺ laser; 9—dye laser; 10—control of ω ; 12—control of magnetic field; 13—control of absorption; 14—control of intensity; 15—balancing of rotation; 16—furnace supplies; 17—control of rotation; 18—control system and analysis of data; PD1 and PD2—photodiodes.

angement enables us to transfer from a given reference point to another in accordance with a preset program, and to detune from the reference point by a given frequency interval.

The furnace is so designed that the bismuth vapor can be introduced into the polarimeter without the use of dividing windows (in way similar to that employed in heat pipes). The internal volume of the polarimeter is filled with helium, and a constant stream of helium flows through the volume at a rate ensuring that the total amount of helium is replaced every few hours. The bismuth vapor is held in a corundum tube, heated to a temperature of about 1200 K by a coaxial niobium heater. A number of reflecting screens are introduced in order to reduce heat transfer by radiation and convection. Metallic bismuth is distributed continuously on the bottom of the corundum tube over a length of about 80 cm. The open ends of the tube are coiled to ensure that the bismuth vapor is condensed, and continuous circulation of the vapor is maintained between the center and the ends, and back again in the liquid form. The furnace is made of copper and is surrounded by a permalloy magnetic screen which reduces the transverse magnetic field down to ≤ 0.002 G. A special coil is placed inside the screen to cancel the Faraday rotation by bismuth vapor in the residual longitudinal field. This coil is also used to produce the calibrated longitudinal magnetic field H_c . The coil configuration is such as to ensure that H_c remains constant to within at least 7% along the entire length of the chamber containing the bismuth vapor. The thermal inertia of the furnace enables us to work for ≤ 10 s with the heater current turned off without affecting κL , so that the magnetic field due to the heater is eliminated during the measurements.

A single-mode light guide is mounted between the laser and the polarimeter to ensure spatial stabilization of the light beam. The analyzing prism of the polarimeter produces spatial separation of the reference and signal beams in such a way that their amplitudes are

$$E_0 = e_0 E_0, \quad E_s = e_s E_s, \quad E_s = \Psi E_0, \quad (9)$$

where e_0 and e_s are the polarization unit vectors; it is assumed that $\Psi \ll 1$ in (7) and (9). The signal beam is intercepted by a photomultiplier and the reference beam by a photodiode.

In principle, the null method of measurement is insensitive to variations in the density $I_0 \propto |E_0|^2$, the modulation amplitude φ_m , the gains in the negative feedback loop, the photocathode sensitivity, and so on. However, rapid intensity fluctuations may produce some additional noise. The noise is suppressed by the analog divider 6 which generates a signal proportional to $|E_c|^2/|E_0|^2$ and used to balance out the rotation $\varphi + \delta(i)$. The negative feedback loop incorporates the following main elements: a narrow-band amplifier, a synchronous detector, an integrator, and a dc amplifier. The current from the amplifier is fed into the control coil of the Faraday modulator. The current is measured by a digital ammeter (so that a long signal-integration time can be used) and is also plotted by a strip charge recorder with a time constant of about 1 s.

The signal from the second divider 7, which is propor-

tional to the transmission of the bismuth vapor, is used to record the absorption spectrum, to monitor the operation of the furnace, and so on. The control system and the analysis of the data rely on a completely automatic measurement of the rotations φ_+ , φ_- , φ_0 in accordance with a preset program. This program monitors the frequency criteria, turns on and off the calibrated magnetic field and the furnace supplies, and performs other calibrations and checks. It also analyzes the results.

INSTRUMENTAL ERRORS

Detailed examination of possible sources of instrumental errors shows that the principal source of difficulty in measuring $\Delta\varphi_{\text{PNC}}$ can be traced to two types of effect, namely, a change in the spatial distribution of intensity in the light beam when the laser frequency is altered, and the interference between the signal beam and scattered light (reflections, flashes, and scattering by surfaces and by defects of the optical elements).

The orientation of the polarization unit vectors of the ordinary and extraordinary waves in the crystal depends on the direction of the wave vector \mathbf{k} . A change in the direction of \mathbf{k} by $\Delta\vartheta$ leads to a spurious rotation $\Delta\varphi$. It can be shown¹¹ that the rotation $\Delta\varphi$ is a minimum when the vector \mathbf{k} is nearly perpendicular to the exit face of the polarizer prism and the entrance face of the analyzer prism. It turns out that

$$\Delta\varphi \approx A\psi\Delta\vartheta + B(\Delta\vartheta)^2, \quad (10)$$

where φ is the angle between the axis of the polarizer crystal and its exit face (for the analyzer—the entrance face), and A , B are coefficients of the order of unity. To reduce $\Delta\varphi$, it is desirable to use prisms with minimum $\psi \lesssim \Delta\vartheta$. Spurious rotation is also produced by any laser-beam displacement and intensity redistribution.

A single-mode light guide is used in the system for the spatial stabilization of the laser beam and to decouple the laser from the polarimeter. The light guide ensures a standard intensity distribution in the emerging beam, which is independent of any changes in the spatial intensity distribution at exit of the light guide.

Figure 2 shows the effect of spatial instability of the laser beam, the dependence of $\Delta\varphi$ on ψ , and the role of the light guide. It also shows to the same scale, the rotation signal in the absence of the bismuth vapor. Figures 2a and b show the rotation at constant wavelength (2a—prisms with ψ of the order of a few degrees, 2b— $\psi \sim 10^{-4}$). Figure 2c corresponds to prisms with $\psi \sim 10^{-4}$ and a periodic linear laser-frequency ramp (repetition frequency 3 GHz) turned on at time t_0 . The results are substantially improved when the light guide is introduced (Figs. 2d, e, f). The null drift at constant laser frequency corresponds to the expected level of shot noise. However, instrumental rotation effects (Fig. 2e) occasionally appear when the frequency is retuned. They can be eliminated by adjusting the polarimeter (Fig. 2f), but eventually reappear again. They are usually much smaller than those shown in Fig. 2e and can only be recorded under signal integration conditions.

These effects can be interpreted as follows. When the reference beam \mathbf{E}_0 is reflected twice or is scattered by optical

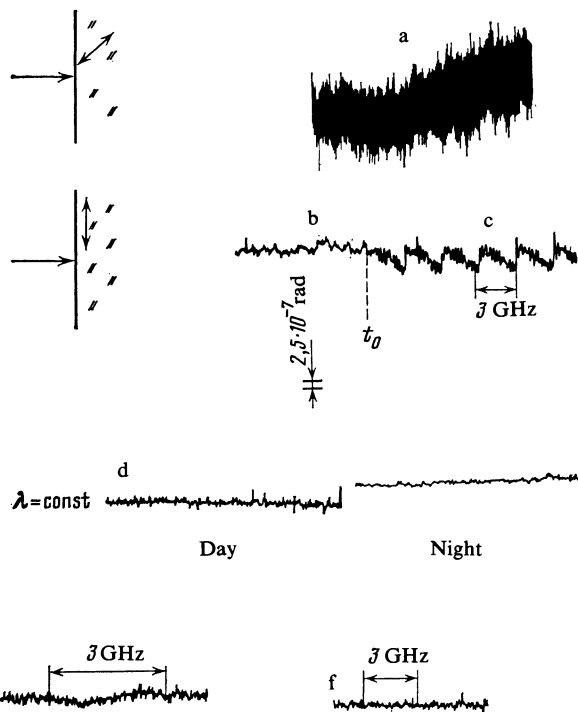


FIG. 2. Recording of spectropolarimeter zero under different conditions. The recording time constant ($\tau \approx 1$ s) and the vertical scale (rotation of the plane of polarization) are the same in all cases.

elements separated by a distance l from one another, the amplitude of \mathbf{E}_0 acquires the additional term

$$e_0 E_0 \alpha e^{2ikh},$$

where α is the product of two amplitude reflection coefficients (scattering coefficients). If partial depolarization is produced, an analogous term appears in the signal component and produces an instrumental rotation

$$\varphi_A = \beta \cos 2kl. \quad (11)$$

When angles in the range $\varphi \sim 10^{-8} - 10^{-7}$ are measured, it is important to take into account possible instrumental errors corresponding to relative intensities of depolarized scattered light of $10^{-14} - 10^{-16}$. The phase of the function in (11), i.e., $2\omega l / c = 4\pi l / \lambda$, changes as the laser frequency ω is returned, and the period Δf (Hz) of the variation in φ_A on the frequency scale is related to the interference baselength l by $\Delta f = c / 2l$. The frequency-dependent instrumental rotation in Fig. 2b corresponds to a path difference $2l$ (or $2ln$) of the order of a few centimeters.

In general, we may have a sum of terms such as (11) with different amplitudes, periods, and phases. The origin of each of these terms can be identified in accordance with its period, i.e., the characteristic interference baselength.

The following steps were taken to suppress possible interference effects. In the fabrication of the optical components, especially the prisms and the Faraday modulator, the quality of the calcite and fused-quartz crystals was carefully controlled. Particular attention was paid to the quality of the surfaces. Surfaces of the optical components were coated to transmit at $\lambda = 648$ nm and were cut in such a way that there were no pairs of parallel faces. Moreover, the polarizer and

analyzer could be displaced by piezoceramic elements, so that the separation l between the optical components of the polarimeter could be modulated, thus averaging out the corresponding interference effects. The modulator was held in a thermostat, so that its optical length could be stabilized either or be varied by varying the temperature.

Our first measurements of $\Delta\varphi_{\text{PNC}}$ were performed^{7,8} at this stage of elimination of possible instrumental errors. Subsequently, most of the attention was devoted to prisms and the Faraday cell, since the path differences corresponding to interference bands within these elements could not be modulated by simple means.

Examination of interference effects introduced by polarimeter prisms shows that the largest errors are due to fabrication defects on the hypotenuse faces of the prisms. For example, a path difference, $k\Delta l n$ is produced in the analyzer prism when the waves E_0, E_s propagate through it, where Δn is the difference between the refractive indices for the ordinary and extraordinary waves. Scattering of the wave E_0 by defects on the exit face produces additional waves that propagate in the direction of the signal wave and back again to the entrance face of the prism. After reflection from the entrance face, the latter waves are also added to the signal wave with the additional phase shift $2kl n$. It is therefore clear that the detector receives both the signal wave $E_s = e_s E_0$ and the waves

$$(e_0\alpha_1 + e_c\beta_1) e^{ikl\Delta n} + (e_0\alpha_2 + e_c\beta_2) e^{i(2kl n + kl\Delta n)}, \quad (12)$$

where the coefficients β_1, β_2 differ from α_1, α_2 by the depolarization factor (corresponding to a reflection or scattering). The result of this is an instrumental rotation

$$\varphi_A = \varphi_{A1} + \varphi_{A2}, \quad (13)$$

$$\varphi_{A1} = \beta_1 \cos(kl\Delta n), \quad \varphi_{A2} = \beta_2 \cos(2kl n + kl\Delta n).$$

More precisely, we have a sum of terms such as (13) with somewhat different values of l for each of the scattering centers. A typical record of the instrumental rotation φ_{A1} is shown in Fig. 3a. For the calcite prism, $\Delta n = 0.17$; the path length l was 0.7 cm, so that the period 250 GHz is in good agreement with the expected value $\Delta f_1 = c/l\Delta n$. The displacement of the laser beam over the prism produces changes in the amplitude, period, and phase of φ_{A1} . The amplitude of φ_{A1} is of the order of 10^{-6} rad, which corresponds to a scattered intensity within the solid angle of the signal beam amounting to about $10^{-12} I_0$. This quantity is a measure of the achieved quality of the prisms. The resultant phase of φ_{A1} can be adjusted relatively easily by adjusting the polarimeter or by varying the temperature so that the maximum or minimum of φ_{A1} occurs at the frequency of the transition under investigation. During this adjustment, the change in φ_{A1} over the 1-GHz interval (separation between maximum and minimum φ_{PNC}) does not exceed 10^{-8} rad. It is also found that the rotation φ_{A1} is quite stable: the characteristic time of variation of the amplitude and phase of this angle is a few hours. This means that the instrumental rotation φ_{A1} imposes practically no restriction on the precisions with which $\Delta\varphi_{\text{PNC}}$ is measured when the above precautions are taken.

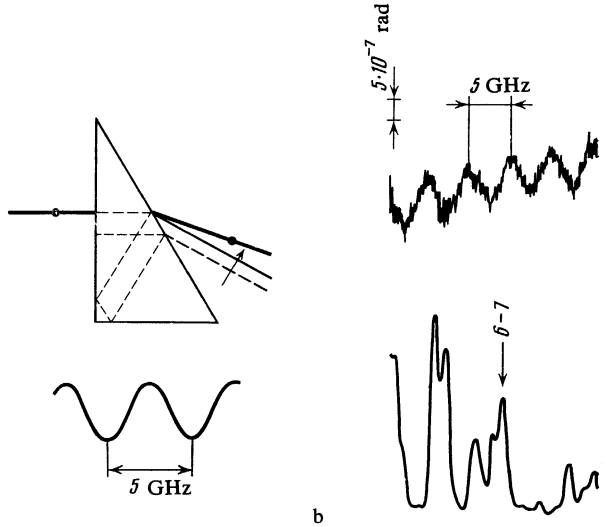
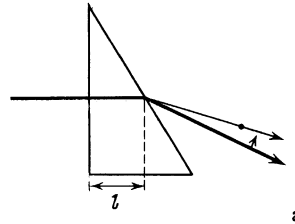
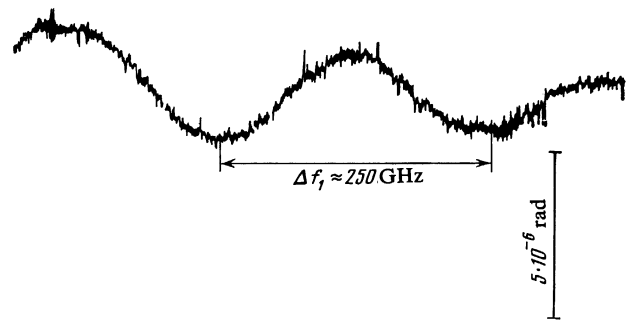


FIG. 3. Instrumental rotation due to interference with the base in the interior of the polarizing (analyzing) prisms: a—spectral dependence of the polarimeter zero in the case of φ_{A1} ; b—simultaneous recording of rotation specially enhanced (by suitable adjustment via interference between beams reflected in the interior of the prism) and of the absorption spectrum of bismuth vapor at $\kappa L \approx 0.1$.

The instrumental effect φ_{A2} is characterized by the much shorter period $\Delta f_2 \approx c/2nl \approx 15$ GHz. It may be expected that $\beta_2 \lesssim 0.1\beta$ (one additional reflection and, furthermore, backward rather than forward scattering). The effect φ_{A2} could not be isolated from noise by a procedure similar to that used for φ_{A1} , but the possibility that it was present could not be ignored. Steps were taken to suppress φ_{A2} when new prisms were fabricated (see below).

Other interference effects can also appear in the prisms due to multiple reflection and scattering with periods $\Delta f \sim 1$ GHz, which is particularly hazardous from our standpoint. Figure 3b shows an example of this type of instrumental effect (specially enhanced). Its period is $\Delta f \approx 5$ GHz.

The following device was adopted to reveal such inter-

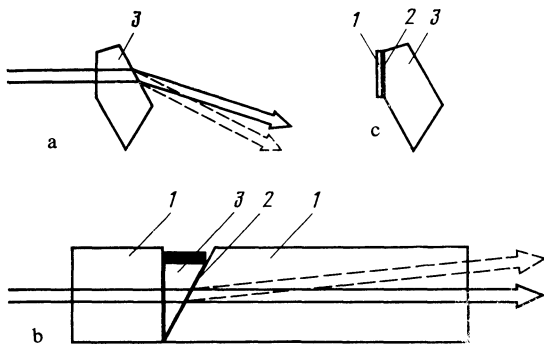


FIG. 4. Different prism (analyzer) designs: 1—optical components made from fused quartz ($n = 1.46$); 2—glycerol immersion ($n = 1.47$); 3—calcite prisms ($n_o = 1.66$; $n_e = 1.48$), refracting angle 30° , optical axis perpendicular to the plane of the drawing and making the angle $\psi \lesssim 10^{-4}$ rad with the entrance face of the prism.

ferences. Waves with polarization \mathbf{e}_0 in (12) do not interfere with the signal wave $\mathbf{E}_s = \mathbf{e}_s E_s$ during detection. If, however, a polarizer with polarization plane at $\pi/4$ to \mathbf{e}_0 is introduced into the beam, an instrumental rotation $\varphi_A = \frac{1}{2}\alpha \cos(\dots)$ is artificially produced. The coefficient α is much greater than the corresponding β . This method was used to amplify and exhibit a number of interference effects and hence trace them back to their sources by determining the interference baselengths.

We have fabricated several sets of prisms and have investigated instrumental rotation due to interference effects in each of them. The design of these prisms is illustrated in Fig. 4. The geometry of the prism shown in Fig. 4a was chosen so as to reduce interference due to multiple reflections. The design of Fig. 4b involves the oil immersion of the prism between two fused-quartz blocks. The aim is to reduce scattering by the hypotenuse and reflection by the entrance faces of the prism. The quartz block has sufficient length to ensure that the signal and reference beams leaving the system are spatially separated. The design of Fig. 4c enables us to achieve a substantial reduction in reflection from the entrance face which carries a thin quartz plate with a high-quality antireflection coating in the form of a glycerol interlayer. High-quality fabrication and transmission of this order could not be achieved for the calcite crystals.

It was found that immersion of the form illustrated in Fig. 4b did not result in a substantial reduction in the amplitude of φ_{A1} with the period of 250 GHz. The best results were obtained with prisms of the form shown in Fig. 4c, and these prisms were subsequently used in all measurements.

Special studies of instrumental uncertainties introduced by the fused quartz rod in the Faraday cell showed that these uncertainties did not exceed 10^{-8} rad when the necessary precautions were taken (choice of material, treatment of ends, inclination of end surfaces, antireflection coating, and thermostating). The uncertainties were simply undetectable. We note that, for our prisms with $\psi \lesssim 10^{-4}$ rad, possible refraction effects in the bismuth vapor cannot produce rotations in excess of 10^{-8} rad.

The frequency-independent instrumental rotation ψ_A should not contribute to $\Delta\varphi_{\text{PNC}} = \varphi_+ - \varphi_-$. If, however,

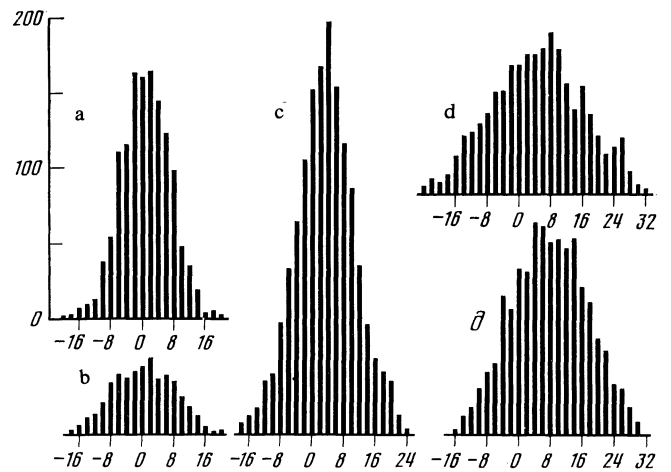


FIG. 5. Histograms of measured values. The rotation of the plane of polarization in units of 10^{-8} rad is shown along the horizontal axis. The vertical axes (all in the same scale) show the number of cycles in which the angle falls into the interval of 2×10^{-8} rad. a—Instrumental zero ($\kappa L = 0$), total number of cycles $\Sigma n_i = 1308$; b— $\kappa L = 0.13$, $\Sigma n_i = 483$; c— $\kappa L = 0.47$, $\Sigma n_i = 2245$; d— $\kappa L = 0.73$, $\Sigma n_i = 1441$; e— $\kappa L = 0.91$, $\Sigma n_i = 1723$.

ψ_A varies with time, the difference $\Delta\varphi_{\text{PNC}}$ may be subject to the uncertainty $\delta\varphi = \varphi_A(t) - \varphi_A(t + \tau)$, where τ is the time between measurements of φ_+ and φ_- . To eliminate the principal part of this uncertainty $(\partial\varphi_A/\partial t)\tau$, which is linear in time, the angles φ_+ , φ_- , φ_0 were measured in the following sequence: $\varphi_0, \varphi_+, \varphi_-; \varphi_0, \varphi_-, \varphi_+; \varphi_0, \varphi_+, \varphi_-; \dots$. Moreover, the measurements were performed for $\tau < 15$ s, which was sufficiently short. The integrating measurements of rotation were made in parallel with plots of the rotation on a strip-charge recorder, so that the instrumental zero drift could be monitored at all times.

We shall not pause here to consider checks made on many other factors such as electrical and magnetic pickup, coupling between control and measuring circuits, shielding of bismuth vapor from magnetic fields at 50, 100, and 1107 Hz, variations in the laser beam intensity, including those that were synchronous with wavelength tuning, and so on.

The final checks on the operation of the system were performed in the integrating mode as follows. The rotation was measured at the three frequency points $\omega_1, \omega_2, \omega_3$, separated by 0.5 GHz and roughly corresponding to the differences $\omega_+ - \omega_0, \omega_0 - \omega_-$. The quantity $\Delta\varphi_A = \varphi_1 - \varphi_3$ was determined. The same procedure was thus adopted as in the measurements of $\Delta\varphi_{\text{PNC}}$. The measurements were performed in the absence of the bismuth vapor within the frequency interval containing the working transition. A set of measurements was also made at reduced bismuth density $\kappa L \approx 0.1$. This was done with reference to the Faraday-rotation zeros $\omega_1 = \omega_+, \omega_3 = \omega_-$.

Figure 5a shows the measured values of $\Delta\varphi_A$ for bismuth. It was found that $\overline{\Delta\varphi_A} = -0.6 \cdot 10^{-8}$ rad. Figure 5b shows a histogram constructed from 483 measurements on the bismuth vapor for $\kappa L = 0.13$. It was found that $\overline{\Delta\varphi_{\text{PNC}}} = -0.4 \cdot 10^{-8}$. The results of a statistical analysis of these measurements will be given below together with measurements of $\Delta\varphi_{\text{PNC}}$ for larger values of κL .

MEASUREMENTS OF $\Delta\varphi_{\text{PNC}}$

One cycle of these measurements involves the determination of rotation at the points $\omega_0, \omega_+, \omega_-$. The sequence of the points ω_+, ω_- is altered in each successive cycle. The measurements were performed in accordance with the following program imposed by the control system: laser frequency adjustment—time T_1 , pause—time T_2 , measurement of rotation—time T_3 . During the time T_1 , the alternating magnetic field (used to adjust the frequency to the corresponding point on the Faraday profile) and the adjustment system and the furnace supplies are turned on and the negative feedback loop in the measurement channel is turned off. During the pause T_2 , the adjustment system, the alternating magnetic field, and the furnace supplies are turned off and the negative feedback loop in the measurement channel is turned on. The measured values are accumulated during the time T_3 . The times T_1, T_2, T_3 could be varied within broad ranges. The difference $\Delta\varphi_{\text{PNC}}$ was measured for $T_1 = 6$, $T_2 = 1.5$, and $T_3 = 6$ s. These values were dictated by the rate of cooling of the furnace when the supplies were turned off. To reduce the time necessary to adjust the laser frequency to the zeros of the Faraday rotation, the frequency was tuned in two stages. First, the data stored in the memory were used to generate a signal for the laser frequency control unit that corresponded to the frequency ω_+ (ω_-) in the preceding cycle, and this was followed by fine tuning.

The stability of the laser frequency during the time T_3 was 35 MHz per cycle and of the order of 8 MHz over 50 cycles. The corresponding uncertainty in the measured $\Delta\varphi_{\text{PNC}} = \varphi_+ - \varphi_-$ did not therefore exceed $0.05\varphi_F^{\text{max}}$ per cycle or $0.01\varphi_F^{\text{max}}$ per 50 cycles, where φ_F^{max} is the maximum Faraday rotation (at the frequency ω_0) in the residual magnetic field. This field was reduced to values corresponding to $\varphi_F^{\text{max}} \leq 10^{-7}$ and was monitored in each cycle.

The difference $\Delta\varphi_{\text{PNC}}$ was measured between June and December 1983 without any modification of the system at three different bismuth vapor pressures corresponding to $\kappa L = 0.91$, $\kappa L = 0.73$, $\kappa L = 0.47$. Control measurements were performed at reduced pressure corresponding to $\kappa L = 0.13$ before each run.

The relatively long furnace enabled us to work at low pressures for which the absorption-line profile was close to the pure Doppler profile. For example, for $\kappa L = 0.91$, the total pressure was 15 Torr and $\gamma/2\Delta\omega_D \leq 0.08$. For other values of κL , the pressure was lower still. The coefficient a in (4) could be determined under these conditions with sufficient precision from the separation between the zeros of the Faraday-rotation profile $\omega_+ - \omega_-$ and $\xi = 1.21$. The differ-

ence $\omega_+ - \omega_-$ was measured to within 1.5–2%. The precision of a was largely determined by the precision with which the ratio $E/2M$ could be determined, and may be estimated at 4–5%.

The calibrated magnetic field H_c necessary to determine κL and to calculate R from $\Delta\varphi_{\text{PNC}}$ [see (3)–(5)] was determined by comparing the Faraday rotation in the quartz rod in a known magnetic field (produced by the long solenoid) and in the field H_c . A check was also made to verify that H_c remained constant along the length of the furnace. The resultant error in all the calibrations, referred to R , does not exceed 10%. Figure 5 shows histograms of the measured $\Delta\varphi_{\text{PNC}}$ for $\kappa L = 0.91, 0.73$, and 0.47 .

Table I lists the results of a χ^2 analysis of the measurements of $\Delta\varphi_{\text{PNC}}$ together with the values of $\omega_+ - \omega_-$ and of the constant a in (4). We calculated the quantity

$$\chi^2 = \sum_{i=1}^m (n_i - r_i)^2 / r_i, \quad (14)$$

where n_i is the number of measurements in the i th interval of values of $\Delta\varphi_{\text{PNC}}$, r_i is the theoretical number for this interval in the case of a Gaussian distribution with parameters $\overline{\Delta\varphi_{\text{PNC}}}$ and σ , and m is the number of intervals. The value of χ^2 given by (14) was minimized with respect to $\overline{\Delta\varphi_{\text{PNC}}}$ and σ . The confidence interval was estimated by using the χ^2 distribution with the number of degrees of freedom $\nu = m - 3$. The confidence interval D at the 90% level was determined from the condition (see Ref. 12).

$$\chi^2(\overline{\Delta\varphi_{\text{PNC}} \pm D, \sigma) = \chi_{\text{min}}^2 + 4.61.$$

It is clear from the values of $\chi_{\text{min}}^2 / \nu$, in Table I and from the shape of the histograms that the distributions of the measured values of $\Delta\varphi_{\text{PNC}}$ do not exhibit large deviations from Gaussian statistics.

Measurements corresponding to different κL were performed for different laser-beam intensities so that the intensity at exit from the polarimeter, after it had been reduced by absorption in bismuth vapor, was roughly at the same level and amounted to a fraction of a milliwatt. The value of σ listed in Table I exceed the values determined by the shot-noise level by not more than factors of 2 or 3.

We may conclude from the data of Table I that our measurements were subject to a small residual instrumental rotation. In some cases, this is found by analyzing the time variation of the measured $\Delta\varphi_{\text{PNC}}$. As an example, Fig. 6 shows four series of measurements for $\kappa L = 0.47$. Each point corresponds to 25 cycles. It is clear that the instrumental rotation oscillates with an amplitude of not more than

TABLE I. Measurements of $\Delta\varphi_{\text{PNC}}$ and their analysis.

κL	$\omega_+ - \omega_-$, MHz	Coefficient a in (4) in units of 10^{-3} rad/G	$\overline{\Delta\varphi_{\text{PNC}}}$, 10^{-8} rad	Confidence interval D (90%) in units of 10^{-8} rad	σ , 10^{-8} rad	$\chi_{\text{min}}^2 / \nu$
0.91	945	0.78	7.70	± 0.55	10	27.5/39
0.73	933	0.81	4.65	± 0.70	12	30/45
0.47	924	0.84	3.15	± 0.35	7.5	25.8/32
0.13	900	0.86	0.40	± 0.80	8.0	18/26
0.0	—	—	0.60	± 0.35	6.0	24/26

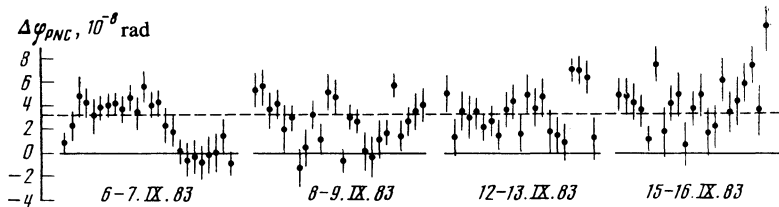


FIG. 6. Chronological sequence of measurements of $\Delta\varphi_{\text{PNC}}$ in series of 25 cycles, each with $\kappa L = 0.47$. The indicated errors correspond to one standard deviation.

3×10^{-8} rad and characteristic times of the order of a few tens of minutes. Analysis of these results shows that these oscillations average out to a level $\leq 10^{-8}$ rad over 500 cycles. Similar conclusions may be drawn from measurements of $\Delta\varphi_A$ ($\kappa L = 0$) and $\Delta\varphi_{\text{PNC}}$ for $\kappa L = 0.13$ (see Table I).

It follows from the foregoing that, under the conditions prevailing in our experiments, the coefficient ξ in (3) was equal to 1.21 and $\Delta\varphi_{\text{PNC}} = -1.08R\kappa L$. The values of $\overline{\Delta\varphi_{\text{PNC}}}(\kappa L)$ deduced from our measurements will be approximated by the following linear formula:

$$\overline{\Delta\varphi_{\text{PNC}}}(\kappa L) = \varepsilon - 1.08R\kappa L, \quad (15)$$

where ε is the residual instrumental rotation. To estimate ε , we shall use measurements of $\Delta\varphi_{\text{PNC}}$ for different κL and measurements of $\Delta\varphi_A$ for $\kappa L = 0$ (without the bismuth vapor).

The uncertainty δR_ε in R can be estimated as follows. It is clear that the uncertainty ε affects R to a lesser extent for larger κL . The value of R deduced from measurements for $\kappa L = 0.91$, assuming $\varepsilon = 0$, is

$$R = (-7.8 \pm 0.55) \cdot 10^{-8}. \quad (16)$$

If we now perform a least-squares determination of R and ε in (15), i.e., minimize the quantity

$$M = \sum_j^N (\Delta\varphi_{\text{PNC}} - \varepsilon + 1.08R\kappa L)^2 / \sigma_j^2 \quad (17)$$

using all the measurement cycles at the points $\kappa L = 0.13$, 0.47, 0.73, and 0.91, we obtain

$$R = (-8.55 \pm 0.35) \cdot 10^{-8}, \quad \varepsilon = -1.15 \cdot 10^{-8}. \quad (18)$$

If the sum over j in (17) includes measurements of the instrumental zero $\Delta\varphi^j$ ($\kappa L = 0$), we find that

$$R = (-7.15 \pm 0.15) \cdot 10^{-8}, \quad \varepsilon = -0.05 \cdot 10^{-8}. \quad (19)$$

It is clear that, in this case, the line $\varepsilon - 1.08R\kappa L$ passes practically through zero.

The quantity δR_ε can be estimated as the maximum

deviation of the values of R in (16), (18), and (19) from the average, i.e., $\delta R_\varepsilon = \pm 0.8 \cdot 10^{-8}$.

The final result for R obtained in the present work may be taken to be the average of the values given by (16), (18), and (19):

$$R = (-7.8 \pm 1.8) \cdot 10^{-8}. \quad (20)$$

The indicated uncertainty of ± 1.8 (in units of 10^{-8}) consists of the statistical uncertainty of 0.2 (1.64 standard deviations for \overline{R}), the instrumental uncertainty $\delta R_\varepsilon = \pm 0.8$, and possible resultant uncertainty of all the calibrations ($\leq 10\%$) $\delta R = \pm 0.8$.

DISCUSSION OF RESULTS

Table II is a summary of all the experimental data on the optical activity of atomic bismuth for the $^4S_{3/2} - ^2D_{3/2}$, $\lambda = 648$ nm transition.

There are several calculations of the constant R . Semiempirical calculations yield

$$R = -18 \cdot 10^{-8} \text{ [Refs. 19, 6]; } R = -16 \cdot 10^{-8} \text{ [Ref. 20].}$$

Hartree-Fock calculations with allowance for electron correlations, yield

$$R = -14 \cdot 10^{-8} \text{ [Refs. 21, 22]; } R = -11 \cdot 10^{-8} \text{ [Ref. 23].}$$

It is clear that our latest results and the results of the Oxford group are in sufficient agreement with one another and with the results of the most detailed calculations.²³

The latest measurements obtained for the $^4S_{3/2} - ^2D_{3/2}$, $\lambda = 876$ nm transition in bismuth are $R_{\text{exp}} = (-10.4 \pm 1.7) \cdot 10^{-8}$ (Refs. 24 and 25) whereas $R_{\text{theor}} = -8.3 \times 10^{-8}$ (Ref. 23). Successful measurements have recently been reported of optical dichroism due to parity nonconservation in thallium²⁶ and cesium,²⁷ and of the optical activity of lead.²⁸

I am greatly indebted to N. G. Basov and M. A. Markov for their attention and support, to E. M. Dianov for providing us with the single-mode light guide, to N. V. Zavaritskiĭ

TABLE II. Measurements of R for the 648-nm line of bismuth by different groups.

Group	year	$R, 10^{-8}$	Reference
Oxford	1977	$+2.7 \pm 4.7$	[13]
Novosibirsk	1978	-19 ± 5	[14]
	1980	-20.2 ± 2.7	[15, 16]
Moscow	1980	-2.4 ± 1.3	[8, 17]
Oxford	1981	-9 ± 2	[18]
Moscow	1984	-7.8 ± 1.8	Present work

for supplying the magnetic screen, and to T. F. Novikova for her major efforts in fabricating the polarizing prisms.

¹The active AZhN-650 liquid was developed and produced at the Research Institute of Organic Intermediate Products and Dyes.

- ¹M. Bouchiat and C. Bouchiat, *Phys. Lett. B* **48**, 111 (1974).
²I. B. Khriplovich, *Pis'ma Zh. Eksp. Teor. Fiz.* **20**, 686 (1974) [*JETP Lett.* **20**, 315 (1974)].
³A. N. Moskalev, R. M. Ryndin, and P. B. Khriplovich, *Usp. Fiz. Nauk* **118**, 409 (1976) [*Sov. Phys. Usp.* **19**, 220 (1976)].
⁴A. A. Alekseev, B. Ya. Zel'dovich, and I. I. Sobel'man, *Usp. Fiz. Nauk* **118**, 385 (1976) [*Sov. Phys. Usp.* **19**, 207 (1976)].
⁵E. N. Fortson and L. Wilets, *Adv. At. Mol. Phys.* **16**, 319 (1980). I. B. Khriplovich, *Nesokhranenie chetnosti v atomnykh yavleniyakh* (Parity Nonconservation in Atomic Phenomena), Nauka, Moscow, 1981.
⁷Yu. V. Bogdanov, I. I. Sobel'man, V. N. Sorokin, and I. I. Struk, *Pis'ma Zh. Eksp. Teor. Fiz.* **31**, 234 (1980) [*JETP Lett.* **31**, 214 (1980)].
⁸Yu. V. Bogdanov, I. I. Sobel'man, V. N. Sorokin, and I. I. Struk, *Pis'ma Zh. Eksp. Teor. Fiz.* **31**, 556 (1980) [*JETP Lett.* **31**, 522 (1980)].
⁹G. J. Roberts, P. E. G. Baird, M. W. S. Brimicombe, *et al.*, *J. Phys. B* **13**, 1389 (1980).
¹⁰D. A. Landman and A. Lurio, *Phys. Rev. A* **1**, 1330 (1970).
¹¹N. B. Baranova, G. N. Birich, Yu. V. Bogdanov, *et al.*, Preprint Nos. 63, 124, FIAN, 1977.
¹²M. Lampton, B. Margon, and S. Bowyer, *Astrophys. J.* **208**, 177 (1976).
¹³P. E. G. Baird, M. W. S. M. Brimicombe, R. G. Hunt, *et al.*, *Phys. Rev. Lett.* **39**, 798 (1977).
¹⁴L. M. Barkov and M. S. Zolotarev, *Pis'ma Zh. Eksp. Teor. Fiz.* **28**, 544 (1978) [*JETP Lett.* **28**, 503 (1978)].
¹⁵L. M. Barkov and M. S. Zolotarev, *Zh. Eksp. Teor. Fiz.* **79**, 713 (1980) [*Sov. Phys. JETP* **52**, 360 (1980)].
¹⁶L. M. Barkov and M. S. Zolotarev, in: *Trudy VII Vavilovskoi konferentsii. Novosibirsk* (Proc. Seventh Vavilov Conference, Novosibirsk), Institute of Automation and Electrometry, Novosibirsk, 1982, Part 1, p. 10.
¹⁷Yu. V. Bogdanov, G. N. Birich, I. I. Sobel'man, V. N. Sorokin, and I. I. Struk, in: *Trudy VII Vavilovskoi konferentsii Novosibirsk* (Proc. Seventh Vavilov Conference, Novosibirsk), 1981, Part 1, p. 17.
¹⁸P. E. G. Baird, R. G. Hunt, L. R. Pendrill, *et al.*, in: *Trudy VII Vavilovskoi konferentsii* (Proc. Seventh Vavilov Conference, Novosibirsk), 1981, Part 1, p. 22.
¹⁹V. N. Novikov, O. P. Sushkov, V. V. Flambaum, and I. B. Kriplovich, *Zh. Eksp. Teor. Fiz.* **71**, 1665 (1976) [*Sov. Phys. JETP* **44**, 872 (1976)].
²⁰D. B. Saakyan, I. I. Sobel'man, and E. A. Yukov, Preprint No. 64, 1980.
²¹M. J. Harris, C. E. Loving, and P. G. H. Sandars, *J. Phys. B* **11**, L749 (1978).
²²P. G. H. Sandars, *Phys. Scripta* **21**, 284 (1980).
²³A. M. Martensson, E. M. Henley, and L. Wilets, *Phys. Rev. A* **24**, 305 (1981).
²⁴E. N. Fortson, in: *Trudy VII Vavilovskoi konferentsii Novosibirsk* (Proc. Seventh Vavilov Conf., Novosibirsk), Novosibirsk, 1981, Part 1, p. 21.
²⁵J. H. Hollister, G. R. Aperson, L. L. Lewis, *et al.*, *Phys. Rev. Lett.* **46**, 643 (1981).
²⁶P. H. Buchsbaum, E. D. Commins, and L. R. Hunter, *Phys. Rev. D* **24**, 1134 (1981).
²⁷M. A. Bouchiat, J. Guena, L. Hunter, and L. Pottier, *Phys. Lett. B* **117**, 258 (1982).
²⁸T. P. Emmons, J. M. Reeves, and E. N. Fortson, *Phys. Rev. Lett.* **51**, 2089 (1983).

Translated by S. Chomet